

3D free-boundary conditions for coordinate-transform finite-difference seismic modelling

Stig Hestholm^{1*} and Bent Ruud²

¹*University of Texas at Dallas, Center for Lithospheric Studies, Mail Station FA31, PO Box 830688, Richardson, TX 75083-0688, USA, and*

²*Department of Solid Earth Physics, University of Bergen, Allgt. 41, 5007 Bergen, Norway*

Received March 2001, revision accepted March 2002

ABSTRACT

New alternative formulations of exact boundary conditions for arbitrary three-dimensional (3D) free-surface topographies on seismic media have been derived. They are shown to be equivalent to previously published formulations, thereby verifying the validity of each set of formulations. The top of a curved grid represents the free-surface topography while the interior of the grid represents the physical medium. We assume the velocity–stress version of the viscoelastic wave equations to be valid in this grid before transforming the equations to a rectangular grid. In order to perform the numerical discretization we apply the latter version of the equations for seismic wave propagation simulation in the medium. The numerical discretization of the free-surface topography boundary conditions by second-order finite differences (FDs) is shown, as well as the spatially unconditional stability of the resulting system of equations. The FD order is increased by two for each point away from the free surface up to eight, which is the order used in the interior. We use staggered grids in both space and time and the second-order leap-frog and Crank–Nicholson methods for wavefield time propagation. An application using parameters typical of teleseismic earthquakes and explosions is presented using a $200 \times 100 \text{ km}^2$ area of real topography from southwestern Norway over a homogeneous medium. A dipping plane wave simulates a teleseismic P-wave incident on the surface topography. Results show conversion from P- to Rg- (short period fundamental mode Rayleigh) waves in the steepest and/or roughest topography, as well as attenuated waves in valleys and fjords. The codes are parallelized for simulation on fast supercomputers and PC-clusters to model high frequencies and/or large areas.

INTRODUCTION

Tessmer and Kosloff (1994) and Tessmer, Kosloff and Behle (1992) transformed the velocity–stress formulation of the elastic wave equations from a curved to a rectangular grid. They applied an iterative treatment to stresses and particle velocities at the surface topography, whereas here we derive explicit, exact conditions for the particle velocities at the free surface, assuming that a curved grid is adapted to this

surface. An immediate advantage of using the velocity–stress formulation is that we do not differentiate material parameters across discontinuities (Virieux 1986). Our method transforms both the internal medium equations (Hestholm 1999) as well as the free-surface boundary conditions from the curved to a rectangular grid where the numerical computations can be performed. The resulting set of boundary conditions is shown to be equivalent to that derived by Hestholm (1999), thus verifying its validity. The resulting equations for the particle velocities at the surface topography are combined with the curved grid wave equations. No extra

*E-mail: stigh@utdallas.edu

memory is needed (except for the topography data) and only marginal extra simulation cost is required compared with the modelling of a free plane surface (Gottschämmer and Olsen 2001). We note that the use of imaging points above the free surface (Levander 1988) is unviable because such methods require a symmetry condition which is not maintained with the introduction of a curved grid. From tests we also found that the use of non-centred FD operators (Fornberg 1988a) for discretization of the boundary conditions leads to instabilities in time. For this reason we have to reduce the FD order near the free surface in order to maintain central, staggered operators. Specifically, at the free surface, second-order FDs have to be used, which do not reduce the modelling accuracy of Rg-waves (Xu, Day and Minster 1999).

DERIVATION OF BOUNDARY CONDITIONS

We define $z_0(\xi, \kappa)$ as any topography function, and a rectangular (ξ, κ, η) -grid bounded by $\xi = 0$, $\xi = \xi_{\max}$ and $\kappa = 0$, $\kappa = \kappa_{\max}$ horizontally and $\eta = 0$ and $\eta = \eta_{\max}$ vertically. We assume a curved grid located in a Cartesian (x, y, z) -coordinate system where the velocity–stress formulation of the viscoelastic wave equations is valid. The extent of the curvature is from a plane at the bottom to where it coincides with any single-valued 3D surface topography function at the top of the grid. Defining

$$A(\xi, \kappa, \eta) \equiv \frac{\partial \eta}{\partial x} = -\frac{\eta}{z_0(\xi, \kappa)} \frac{\partial z_0(\xi, \kappa)}{\partial \xi}, \quad (1)$$

$$B(\xi, \kappa, \eta) \equiv \frac{\partial \eta}{\partial y} = -\frac{\eta}{z_0(\xi, \kappa)} \frac{\partial z_0(\xi, \kappa)}{\partial \kappa}, \quad (2)$$

$$C(\xi, \kappa) \equiv \frac{\partial \eta}{\partial z} = \frac{\eta_{\max}}{z_0(\xi, \kappa)}, \quad (3)$$

the equations for the stresses in the velocity–stress formulation of the viscoelastic curved grid wave equations with one relaxation mechanism (or standard linear solid (SLS)), given in the rectangular (ξ, κ, η) -grid (Hestholm 1999), can be written,

$$\begin{aligned} \frac{\partial \sigma_{ii}}{\partial t} &= \Pi \frac{\tau_e^P}{\tau_\sigma} \left(\sum_{k=1}^2 \frac{\partial u_k}{\partial \xi_k} + \sum_{k=1}^3 A_k(\xi, \kappa, \eta) \frac{\partial u_k}{\partial \eta} \right) \\ &\quad - 2\mu \frac{\tau_e^S}{\tau_\sigma} \left(\sum_{k=1, k \neq i}^2 \frac{\partial u_k}{\partial \xi_k} + \sum_{k=1, k \neq i}^3 A_k(\xi, \kappa, \eta) \frac{\partial u_k}{\partial \eta} \right) + r_{ii}, \end{aligned} \quad (4)$$

$$\begin{aligned} \frac{\partial \sigma_{ij}}{\partial t} &= \mu \frac{\tau_e^S}{\tau_\sigma} \left(\frac{\partial u_i}{\partial \xi_j, j \neq 3} + \frac{\partial u_j}{\partial \xi_i, i \neq 3} + A_i(\xi, \kappa, \eta) \frac{\partial u_j}{\partial \eta} + A_j(\xi, \kappa, \eta) \frac{\partial u_i}{\partial \eta} \right) + r_{ij}, \end{aligned} \quad (5)$$

where $\xi_{k, k=1, 2, 3} = (\xi, \kappa, \eta)$ and $A_{k, k=1, 2, 3}(\xi, \kappa, \eta) = (A(\xi, \kappa, \eta), B(\xi, \kappa, \eta), C(\xi, \kappa))$. Π is the relaxation modulus for P-waves, $\Pi = \lambda + 2\mu$ (λ and μ are the Lamé parameters), and μ is the relaxation modulus for S-waves as in the elastic case. τ_e^P and τ_e^S are the strain relaxation times for P- and S-waves, respectively, and τ_σ is the stress relaxation time. The same τ_σ can be used both for P- and S-waves (Blanch, Robertsson and Symes 1995). $\sigma_{ij}; i, j = 1, 2, 3$, are the six stress components and $r_{ij}; i, j = 1, 2, 3$, are the six memory variable components in viscoelastic modelling, using one SLS. $u_i; i = 1, 2, 3 = (u, v, w)$ are the particle velocity components.

The boundary condition at any free surface is that the traction vector T vanishes,

$$T \equiv \tau \cdot n = 0, \quad (6)$$

i.e. in Cartesian coordinates,

$$\sigma_{ij} n_j = 0, \quad (7)$$

where τ is the stress tensor with components σ_{ij} and n is a normal vector to the local surface point with components n_j ; $i, j = 1, 2, 3$. Any normal vector may be used, even though T is defined by the unit normal vector. In 3D we can choose

$$n = \left(-\frac{\partial z_0(\xi, \kappa)}{\partial \xi}, -\frac{\partial z_0(\xi, \kappa)}{\partial \kappa}, 1 \right)^T = (-b_x, -b_y, 1)^T, \quad (8)$$

with $b_x = \partial z_0(\xi, \kappa)/\partial \xi$ and $b_y = \partial z_0(\xi, \kappa)/\partial \kappa$, b being the elevation data function and index T indicating transpose. Partially differentiating (7) with respect to time and using the given n yields

$$-b_x \frac{\partial \sigma_{xx}}{\partial t} - b_y \frac{\partial \sigma_{xy}}{\partial t} + \frac{\partial \sigma_{xz}}{\partial t} = 0, \quad (9)$$

$$-b_x \frac{\partial \sigma_{xy}}{\partial t} - b_y \frac{\partial \sigma_{yy}}{\partial t} + \frac{\partial \sigma_{yz}}{\partial t} = 0, \quad (10)$$

$$-b_x \frac{\partial \sigma_{xz}}{\partial t} - b_y \frac{\partial \sigma_{yz}}{\partial t} + \frac{\partial \sigma_{zz}}{\partial t} = 0, \quad (11)$$

with σ_{xx} , σ_{xy} , σ_{yy} , σ_{xz} , σ_{yz} and σ_{zz} being the stress components. We now substitute the expressions for all time-differentiated stresses from (4) and (5), noting that the limit of an elastic medium can be assumed at the surface (Robertsson 1996). Therefore $\tau_e \equiv \tau_\sigma$ for both P- and S-waves and the memory variables vanish, i.e. $r_{ij} \equiv 0$; $i, j = 1, 2, 3$. Furthermore, using the properties from (1)–(3), valid at the surface: $A(\xi, \kappa, \eta) = -C(\xi, \kappa)b_x$,

$$A(\xi, \kappa, \eta) = -C(\xi, \kappa)b_y, \quad (13)$$

and rearranging terms, we obtain the following form of (9)–(11):

$$\begin{aligned} & \left[b_x^2(\lambda + 2\mu) + \mu(1 + b_y^2) \right] C(\xi, \kappa) \frac{\partial u}{\partial \eta} + b_x b_y (\lambda + \mu) C(\xi, \kappa) \frac{\partial v}{\partial \eta} \\ & - b_x (\lambda + \mu) C(\xi, \kappa) \frac{\partial w}{\partial \eta} \\ = & b_x (\lambda + 2\mu) \frac{\partial u}{\partial \xi} + b_y \mu \frac{\partial v}{\partial \xi} - \mu \frac{\partial w}{\partial \xi} + b_y \mu \frac{\partial u}{\partial \kappa} + b_x \lambda \frac{\partial v}{\partial \kappa}, \end{aligned} \quad (14)$$

$$\begin{aligned} & b_x b_y (\lambda + \mu) C(\xi, \kappa) \frac{\partial u}{\partial \eta} + \left[\mu(1 + b_x^2) + b_y^2(\lambda + 2\mu) \right] C(\xi, \kappa) \frac{\partial v}{\partial \eta} \\ & - b_y (\lambda + \mu) C(\xi, \kappa) \frac{\partial w}{\partial \eta} \\ = & b_y \lambda \frac{\partial u}{\partial \xi} + b_x \mu \frac{\partial v}{\partial \xi} + b_x \mu \frac{\partial u}{\partial \kappa} + b_y (\lambda + 2\mu) \frac{\partial v}{\partial \kappa} - \mu \frac{\partial w}{\partial \kappa}, \end{aligned} \quad (15)$$

$$\begin{aligned} & - b_x (\lambda + \mu) C(\xi, \kappa) \frac{\partial u}{\partial \eta} - b_y (\lambda + \mu) C(\xi, \kappa) \frac{\partial v}{\partial \eta} \\ & + \left[(\lambda + 2\mu) + \mu(b_x^2 + b_y^2) \right] C(\xi, \kappa) \frac{\partial w}{\partial \eta} \\ = & -\lambda \frac{\partial u}{\partial \xi} + b_x \mu \frac{\partial w}{\partial \xi} - \lambda \frac{\partial v}{\partial \kappa} + b_y \mu \frac{\partial w}{\partial \kappa}. \end{aligned} \quad (16)$$

We introduce the definitions,

$$\zeta \equiv \frac{\lambda}{\lambda + 2\mu},$$

$$d \equiv b_x = \frac{\partial z_0(\xi, \kappa)}{\partial \xi} = \tan \theta,$$

$$e \equiv \cos [\arctan(d)] = \cos \theta,$$

$$f \equiv \sin [\arctan(d)] = \sin \theta, \quad (20)$$

$$p \equiv b_y e = \frac{\partial z_0(\xi, \kappa)}{\partial \kappa} e = \tan \phi, \quad (21)$$

where θ and ϕ are slope angles of the local topography with the horizontal. Multiplying (14)–(16) by $2/(\lambda + 2\mu)$ and noting that

$$\frac{\mu}{\lambda + 2\mu} = \frac{\frac{1}{2}(\lambda + 2\mu - \lambda)}{\lambda + 2\mu} = \frac{1}{2}(1 - \zeta), \quad (22)$$

and hence

$$\frac{\lambda + \mu}{\lambda + 2\mu} = \zeta + \frac{1}{2}(1 - \zeta) = \frac{1}{2}(1 + \zeta), \quad (23)$$

we obtain the boundary conditions (14)–(16) in the form:

$$\begin{aligned} & \left[2d^2 + (1 - \zeta) \left(1 + \frac{p^2}{e^2} \right) \right] C(\xi, \kappa) \frac{\partial u}{\partial \eta} + \frac{dp}{e} (1 + \zeta) C(\xi, \kappa) \frac{\partial v}{\partial \eta} \\ & - d(1 + \zeta) C(\xi, \kappa) \frac{\partial w}{\partial \eta} \\ = & 2d \frac{\partial u}{\partial \xi} + \frac{p}{e} (1 - \zeta) \frac{\partial v}{\partial \xi} - (1 - \zeta) \frac{\partial w}{\partial \xi} + \frac{p}{e} (1 - \zeta) \frac{\partial u}{\partial \kappa} + 2d \zeta \frac{\partial v}{\partial \kappa}, \end{aligned} \quad (24)$$

$$\begin{aligned} & \frac{dp}{e} (1 + \zeta) C(\xi, \kappa) \frac{\partial u}{\partial \eta} + \left[(1 - \zeta)(1 + d^2) + 2 \frac{p^2}{e^2} \right] C(\xi, \kappa) \frac{\partial v}{\partial \eta} \\ & - \frac{p}{e} (1 + \zeta) C(\xi, \kappa) \frac{\partial w}{\partial \eta} \\ = & 2 \frac{p}{e} \zeta \frac{\partial u}{\partial \xi} + d(1 - \zeta) \frac{\partial v}{\partial \xi} + d(1 - \zeta) \frac{\partial u}{\partial \kappa} + 2 \frac{p}{e} \frac{\partial v}{\partial \kappa} - (1 - \zeta) \frac{\partial w}{\partial \kappa}, \end{aligned} \quad (25)$$

$$\begin{aligned} & - d(1 + \zeta) C(\xi, \kappa) \frac{\partial u}{\partial \eta} - \frac{p}{e} (1 + \zeta) C(\xi, \kappa) \frac{\partial v}{\partial \eta} \\ & + \left[2 + (1 - \zeta) \left(d^2 + \frac{p^2}{e^2} \right) \right] C(\xi, \kappa) \frac{\partial w}{\partial \eta} \\ = & -2\zeta \frac{\partial u}{\partial \xi} + d(1 - \zeta) \frac{\partial w}{\partial \xi} - 2\zeta \frac{\partial v}{\partial \kappa} + \frac{p}{e} (1 - \zeta) \frac{\partial w}{\partial \kappa}. \end{aligned} \quad (26)$$

The Appendix shows that these conditions are equivalent to the boundary condition formulations derived by Hestholm (1999), i.e.

$$\begin{aligned} & \frac{1}{e^2} (1 + p^2) C(\xi, \kappa) \frac{\partial u}{\partial \eta} + \frac{d}{e^2} (1 + p^2) C(\xi, \kappa) \frac{\partial w}{\partial \eta} \\ = & 2d \frac{\partial u}{\partial \xi} + \frac{p}{e} \frac{\partial v}{\partial \xi} + (d^2 - 1) \frac{\partial w}{\partial \xi} + \frac{p}{e} \frac{\partial u}{\partial \kappa} + \frac{dp}{e} \frac{\partial w}{\partial \kappa}, \end{aligned} \quad (27)$$

$$\begin{aligned} & - \frac{fp}{e^2} (1 + p^2) C(\xi, \kappa) \frac{\partial u}{\partial \eta} + \frac{1}{e^2} (1 + p^2) C(\xi, \kappa) \frac{\partial v}{\partial \eta} \\ & + \frac{p}{e} (1 + p^2) C(\xi, \kappa) \frac{\partial w}{\partial \eta} \end{aligned} \quad (18)$$

$$\begin{aligned} = & -2dfp \frac{\partial u}{\partial \xi} + d(1 - p^2) \frac{\partial v}{\partial \xi} + 2fp \frac{\partial w}{\partial \xi} + d(1 - p^2) \frac{\partial u}{\partial \kappa} \\ & + 2 \frac{p}{e} \frac{\partial v}{\partial \kappa} + (p^2 - 1) \frac{\partial w}{\partial \kappa}, \end{aligned} \quad (28)$$

$$\begin{aligned} & \frac{d}{e^2} (1 + p^2) C(\xi, \kappa) \frac{\partial u}{\partial \eta} + \frac{p}{e^3} (1 + p^2) C(\xi, \kappa) \frac{\partial v}{\partial \eta} \\ & - \frac{1}{e^2} (1 + p^2) C(\xi, \kappa) \frac{\partial w}{\partial \eta} \\ = & \left[\zeta \left(1 + \frac{p^2}{e^2} \right) + d^2 \right] \frac{\partial u}{\partial \xi} - \frac{dp}{e} (\zeta - 1) \frac{\partial v}{\partial \xi} + d(\zeta - 1) \frac{\partial w}{\partial \xi} \\ & - \frac{dp}{e} (\zeta - 1) \frac{\partial u}{\partial \kappa} + \frac{1}{e^2} (\zeta + p^2) \frac{\partial v}{\partial \kappa} + \frac{p}{e} (\zeta - 1) \frac{\partial w}{\partial \kappa}, \end{aligned} \quad (29)$$

again using definitions (3) and (17)–(21). Both forms (14)–(16) (alternatively (24)–(26)) and (27)–(29) are closed, exact systems of equations for the particle velocities at a surface topography. In the derivation of both forms, $\mu \neq 0$ is assumed. This means that the conditions cannot be used exactly for acoustic cases. Neither can they be used for vertical subsections, since $\tan \theta$ and/or $\tan \phi$ then tend to infinity. Under these constraints, both systems of equations are spatially unconditionally stable when discretized by second-order FDs. We show this fact in the next section for the set (27)–(29). For the set (14)–(16), this is easily shown for the

special cases $b_x = 0$ and $b_y = 0$. Therefore it is always true, due to the fact that the determinant of a system of equations is invariant under rotation of the coordinate system. Our experiments show that the forms (14)–(16) and (27)–(29) exhibit the same numerical properties in simulations. The derivation of the new set (14)–(16) and its equivalence to the form (27)–(29) (see Appendix) serves mainly as a simpler derivation and a verification of the previous form. We use the form (27)–(29) for the numerical example in this paper.

Using definitions (17)–(21), we define

$$\begin{aligned}\gamma_{11} &\equiv \frac{1}{e^2}, & \gamma_{12} &\equiv 0, & \gamma_{13} &\equiv \frac{d}{e^2}, \\ \gamma_{21} &\equiv -\frac{fp}{e^2}, & \gamma_{22} &\equiv \frac{1}{e^2}, & \gamma_{23} &\equiv \frac{p}{e},\end{aligned}\quad (30)$$

$$\gamma_{31} \equiv -\frac{d}{e^2}, \quad \gamma_{32} \equiv -\frac{p}{e^3}, \quad \gamma_{33} \equiv \frac{1}{e^2}, \quad (31)$$

$$\alpha_{11} \equiv 2d, \quad \alpha_{12} \equiv \frac{p}{e}, \quad \alpha_{13} \equiv d^2 - 1, \quad (32)$$

$$\alpha_{21} \equiv -2dfp, \quad \alpha_{22} \equiv d(1 - p^2), \quad \alpha_{23} \equiv 2fp, \quad (33)$$

$$\begin{aligned}\alpha_{31} &\equiv -\left[\zeta\left(1 + \frac{p^2}{e^2}\right) + d^2\right], & \alpha_{32} &\equiv \frac{dp}{e}(\zeta - 1), \\ \alpha_{33} &\equiv -d(\zeta - 1),\end{aligned}\quad (34)$$

$$\beta_{11} \equiv \frac{p}{e}, \quad \beta_{12} \equiv 0, \quad \beta_{13} \equiv \frac{dp}{e}, \quad (35)$$

$$\beta_{21} \equiv d(1 - p^2), \quad \beta_{22} \equiv 2\frac{p}{e}, \quad \beta_{23} \equiv p^2 - 1, \quad (36)$$

$$\beta_{31} \equiv \frac{dp}{e}(\zeta - 1), \quad \beta_{32} \equiv -\frac{1}{e^2}(\zeta + p^2), \quad \beta_{33} \equiv -\frac{p}{e}(\zeta - 1). \quad (37)$$

Then the topography boundary conditions (27)–(29) can be written

$$\gamma(1 + p^2) C(\xi, \kappa) \begin{pmatrix} \partial u / \partial \eta \\ \partial v / \partial \eta \\ \partial w / \partial \eta \end{pmatrix} = \boldsymbol{\alpha} \begin{pmatrix} \partial u / \partial \xi \\ \partial v / \partial \xi \\ \partial w / \partial \xi \end{pmatrix} + \boldsymbol{\beta} \begin{pmatrix} \partial u / \partial \kappa \\ \partial v / \partial \kappa \\ \partial w / \partial \kappa \end{pmatrix}, \quad (38)$$

using definition (3), and γ is the 3×3 matrix consisting of the elements γ_{lm} , $\boldsymbol{\alpha}$ is the 3×3 matrix consisting of the elements α_{lm} , and $\boldsymbol{\beta}$ is the 3×3 matrix consisting of the elements β_{lm} .

NUMERICAL DISCRETIZATION

We discretize the boundary condition (38) for the particle velocities at the surface by second-order, staggered FDs. The discretized version becomes

$$\begin{aligned}& \gamma(1 + p^2) C(\xi, \kappa) \frac{1}{dz} \begin{pmatrix} [u(i, j, k) - u(i, j, k - 1)] \\ [v(i, j, k) - v(i, j, k - 1)] \\ [w(i, j, k) - w(i, j, k - 1)] \end{pmatrix} \\ &= \boldsymbol{\alpha} \frac{1}{dx} \begin{pmatrix} [u(i, j, k - 1) - u(i - 1, j, k - 1)] \\ [v(i, j, k - 1) - v(i - 1, j, k - 1)] \\ [w(i, j, k - 1) - w(i - 1, j, k - 1)] \end{pmatrix} \\ &+ \boldsymbol{\beta} \frac{1}{dy} \begin{pmatrix} [u(i, j, k - 1) - u(i, j - 1, k - 1)] \\ [v(i, j, k - 1) - v(i, j - 1, k - 1)] \\ [w(i, j, k - 1) - w(i, j - 1, k - 1)] \end{pmatrix},\end{aligned}\quad (39)$$

where k is taken to be the level of the surface topography; here k denotes the vertical index and i and j the first and second horizontal indices, respectively. dz is the vertical grid distance of the numerical mesh, whereas dx and dy are the first and second horizontal grid distances. $u(i, j, k - 1)$, $v(i, j, k - 1)$, $w(i, j, k - 1)$, $u(i - 1, j, k - 1)$, $v(i - 1, j, k - 1)$, $w(i - 1, j, k - 1)$, $u(i, j - 1, k - 1)$, $v(i, j - 1, k - 1)$ and $w(i, j - 1, k - 1)$ are all known from calculations from the interior medium equations. We solve this system with respect to $u(i, j, k)$, $v(i, j, k)$ and $w(i, j, k)$, which are the surface values of the particle velocities. This gives a closed, explicit system of equations with determinant

$$\begin{aligned}D &= [\det \gamma](1 + p^2)^3 C^3(\xi, \kappa) \\ &= \frac{1}{e^6} (1 + p^2)^4 (1 + d^2) C^3(\xi, \kappa) > 0, \quad \forall \theta, \forall \phi.\end{aligned}\quad (40)$$

This determinant is always positive for all slope angles θ and ϕ and its minimum value is $C^3(\xi, \kappa)$, which occurs for a plane surface. Therefore the solution of (39) is unconditionally stable. This spatial stability is more important than might be realized. The reason is that the numerical dispersion of the phase velocity of Rg-waves is of the same order, regardless of the FD order used or whether the pseudospectral method (Fornberg 1988b) is used for spatial differentiation. Only modelling of body waves gains in accuracy when high-order FD or pseudospectral methods are applied (Xu *et al.* 1999). This means that the numerical dispersion of Rg-waves can only be reduced by closer spatial sampling regardless of modelling order. As a result the second-order FD method should be used since it is the most cost-effective. For numerical discretization of the interior viscoelastic wave equations we refer to the corresponding sections in Hestholm (1999) and Ruud and Hestholm (2001).

P- TO RG-SCATTERING FROM A FJORD TOPOGRAPHY

Figure 1 shows the elevation (upper map) and gradients (lower map) of a $200 \times 100 \text{ km}^2$ coastal area of topography in southwestern Norway with the city of Bergen at about $x = 50, y = 50 \text{ km}$. Generally, elevation increases towards the east of the area with the steepest gradients centred around the middle of the west–east direction. The edges of the long and prominent Hardangerfjord, incising the middle of the area from the south, contain the steepest and fastest varying gradients of the map. We simulate an initial dipping plane wave representing incident teleseismic P-waves travelling towards the area. The plane wave arrives from northwest. Its angle of incidence with the west–east direction (x -axis) is 1.79° (a negative slope of $1/32$) and with the south–north direction (y -axis), it is 3.58° (a positive slope of $1/16$). This situation is shown in Fig. 2 at times 1.7 s and 2.9 s after the initial excitation. The initial plane wave approaches the surface topography and is implemented as a plane of Ricker point sources, each source having a central frequency of 2.5 Hz. The homogeneous medium has $v_p = 6.0 \text{ km/s}$, $v_s = 3.46 \text{ km/s}$, density = 2000 kg/m^3 , $Q_p = 250$ and $Q_s = 200$. A total grid size of $1000 \times 500 \times 150$ is used with a uniform grid sampling of 0.2 km , thus the model is 30 km deep. The total time simulated is 6.5 s. Message passing interface (MPI) was used to parallelize the program code by domain decomposition. The simulation took approximately 6 hours using a total of 8.1 GB on 32 processors on the parallel SGI (Cray) Origin 2000 machine located at Parallab, University of Bergen, Norway.

Surface topography views of the development of the vertical particle velocity component across the coastal topography were taken at intervals of 1.2 s. Figure 2 shows views at 1.7 s and 2.9 s. The procedure for absorption along grid boundaries is seen to work well. The medium is homogeneous, which means that the fjords and the sea are modelled as solid earth with the same medium properties as the rest of the model. Simulation of seismic/acoustic interfaces is possible using the program code with simpler media because, even if $\mu \neq 0$ is assumed in the derivation of the boundary conditions, we do not divide by μ anywhere in the numerical implementation. However, the complex fjord landscape of the present simulation leads to instabilities when applying high-order FD operators across water-filled fjords.

The effects of the Hardangerfjord on the wavefield are clearly visible across the middle of the area in the south–north direction in Fig. 2. We confirm that the steepest and

roughest topography, as seen in the lower half of Fig. 1, gives rise to the strongest wavefield amplitudes in Fig. 2. This is verified from the broad south–north orientated complex waveband of strong amplitudes in Fig. 2. Since plot scales are relative to amplitude strength, the strongest amplitudes of the simulation are displayed as clear blue/red contrasts, even if scattering exists in the entire domain with the exception of the far west. A multiplicity of scattered waves can be observed. Circular wave patterns are confirmed around the locations of strongest gradients and topography variations.

Figure 3 shows the next two views of the development of the vertical particle velocity component across the coastal topography, i.e. at 4.1 s and 5.3 s. Here it is possible to follow the scattered waves from the previous snapshots with time and identify the strongest scattering sources as located close to and inside the sharp red and blue wavefronts. Scattering is caused solely by surface topography since the medium is homogeneous. A great amount of scattering in the present example is due to out-of-plane effects from 3D topography, because 2D synthetics lead to much simpler seismograms (Hestholm, Ruud and Husebye 1999). Some grid boundary reflections are seen to interfere with the scattering in all the snapshots. In this regard, the present situation of a plane wave reaching all grid edges is a worst case scenario because wave components in all directions reach all grid edges immediately.

Topography profiles across the model's west–east direction (upper part) and south–north direction (lower part) are shown in Fig. 4. Each profile is taken at the middle point of the model. Horizontal axes are in kilometres and vertical axes are in 100 m, so in effect vertical axes are stretched 10 times compared with horizontal axes, thus emphasizing topographic variations across the domain. Receivers are located from 76 to 125 km along the west–east profile and from 26 to 75 km along the south–north profile. Figure 5 shows seismograms of the vertical particle velocity component w at 50 receivers spaced at 1 km intervals along the west–east profile. Clearly, we see that the mountain from 75 km to about 95 km generates a continuous and complex wavetrain of Rg-waves away from it. We see from both topography profiles (Fig. 4) that the two features of strong gradients and topographic variations are coincident, resulting in a complicated pattern of Rg-waves in Fig. 5. Also the presence of scattering effects from nearby out-of-plane topographic features that enhance the seismogram's complex appearance can be seen. Fjords are seen to be the areas of least scattering and they attenuate higher frequencies of scattered waves propagating towards them. In Fig. 5 this is seen between receivers 30 and 40 and

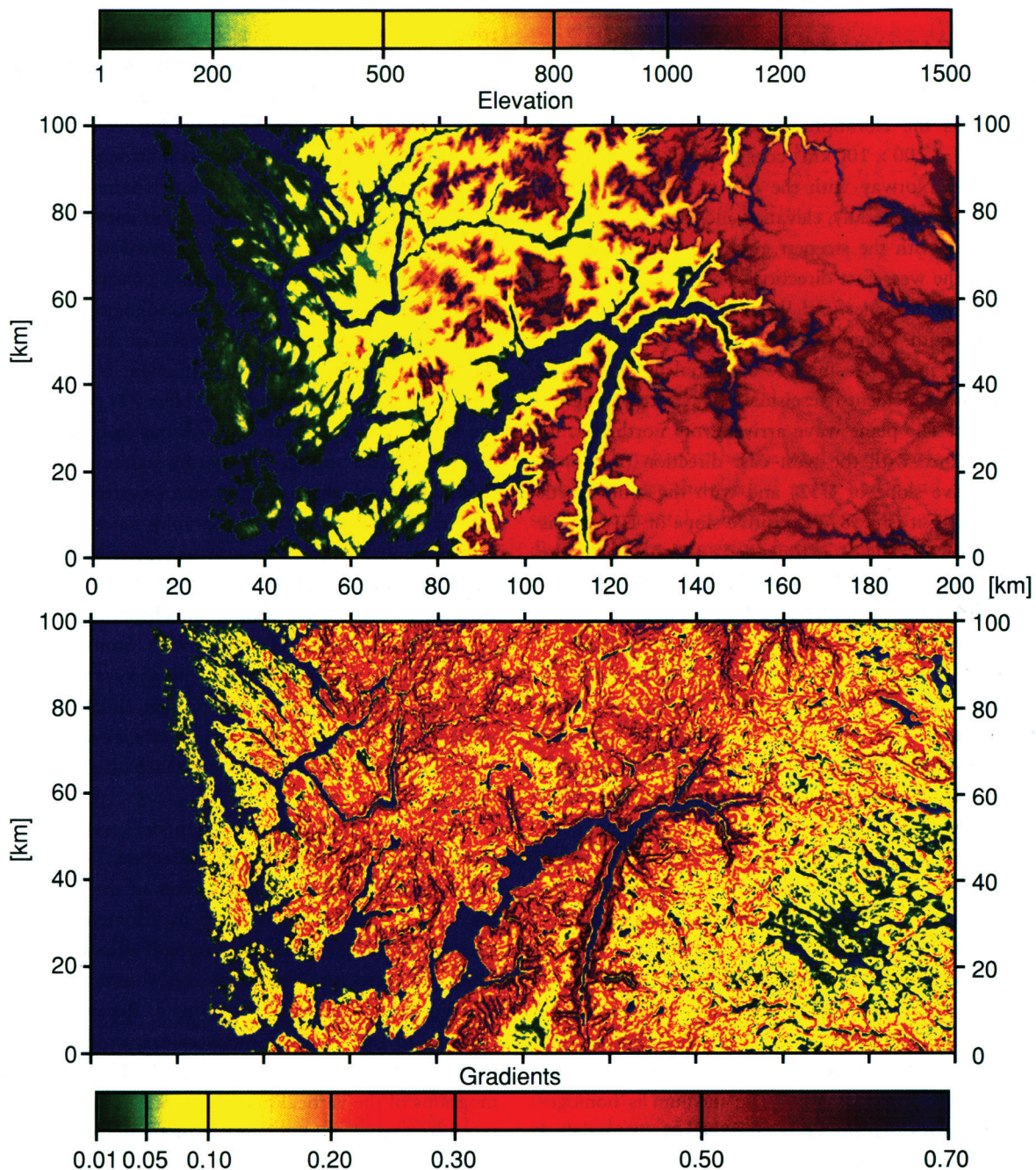


Figure 1 Upper map: Elevation data of the $200 \times 100 \times 30 \text{ km}^3$ domain used in the 3D simulation. The seismogram receivers are spaced at 1 km intervals and are located along two profiles: from 76 to 125 km in the west–east (x) direction at $y=50 \text{ km}$ and from 26 to 75 km in the south–north (y) direction at $x=100 \text{ km}$. Labels are in kilometres and blue represents zero values. Lower map: Gradients of the area; blue represents zero values.

from 48 onwards. Such features are also seen on the u - and v -components (not shown).

Figure 6 shows seismograms along the south–north profile of Fig. 4 (lower part) taken at 50 receivers, located at intervals of 1 km, for the horizontal particle velocity

component u . The seismograms show complex scattering from the mountainous features; it is possible to identify these features as the sources of strongest amplitudes of incoherent scattering. The u -component is the transverse component of the profile. Therefore, it is natural that this

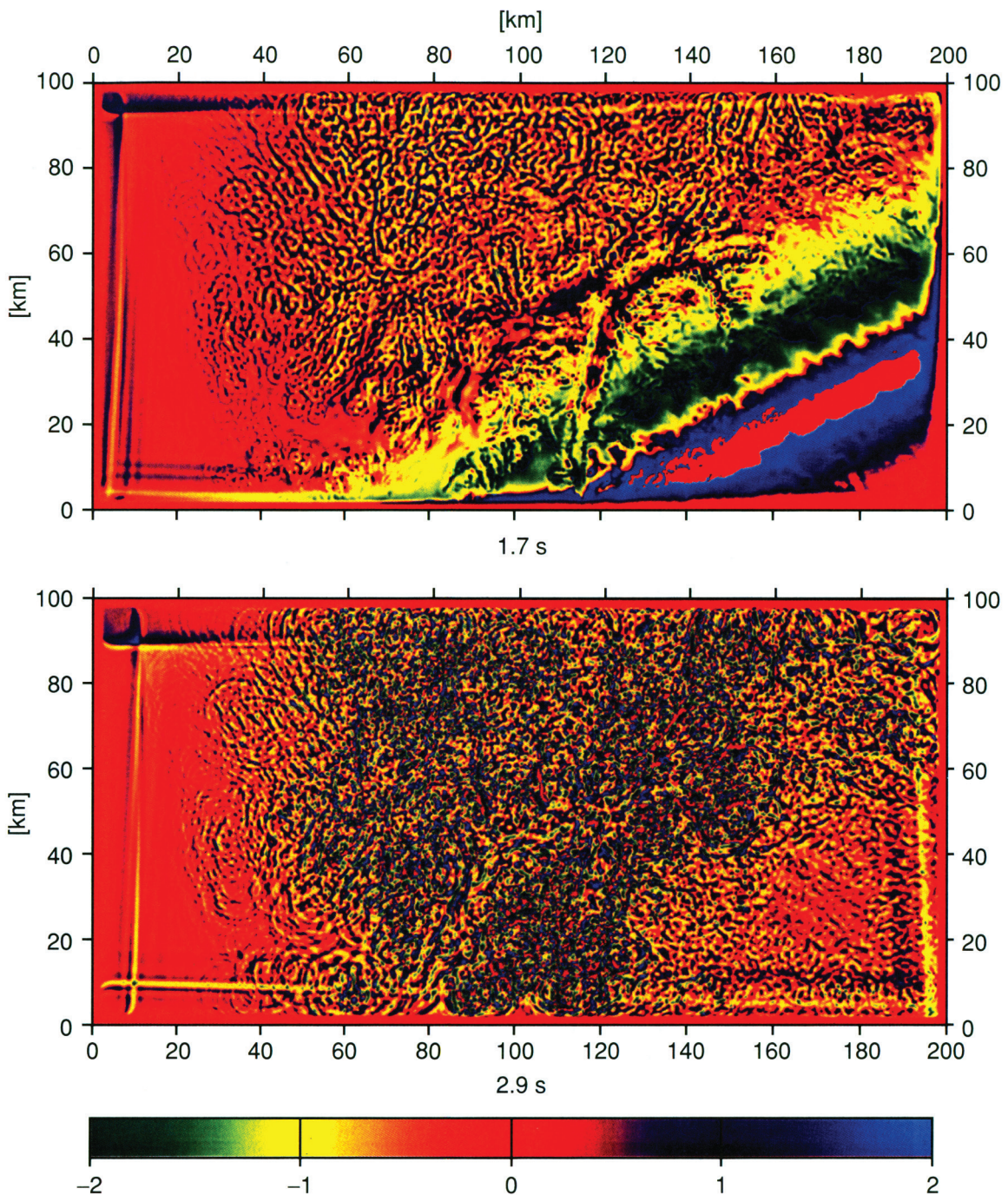


Figure 2 Snapshots of the vertical particle velocity component w at times 1.7 s and 2.9 s after a dipping plane wave is released close to the northwest corner of the surface topography of Fig. 1. The dip of the plane wave is 1/32 in the negative x -direction and 1/16 in the positive y -direction. The snapshots of the viscoelastic simulation are taken along the surface topography of Fig. 1 using a homogeneous medium of $Q_P = 250$, $Q_S = 200$, $v_P = 6 \text{ km/s}$, $v_S = 3.46 \text{ km/s}$ and density = 2000 kg/cm^3 .

component is attenuated significantly in the fjord between 40 km and 50 km (between receivers 14 and 20), the fjord acting as a valley. For the component v parallel to the profile

(not shown), on the other hand, there are strong Rg-waves propagating northwards into the fjord caused by the complicated topographic features to the south of the fjord.

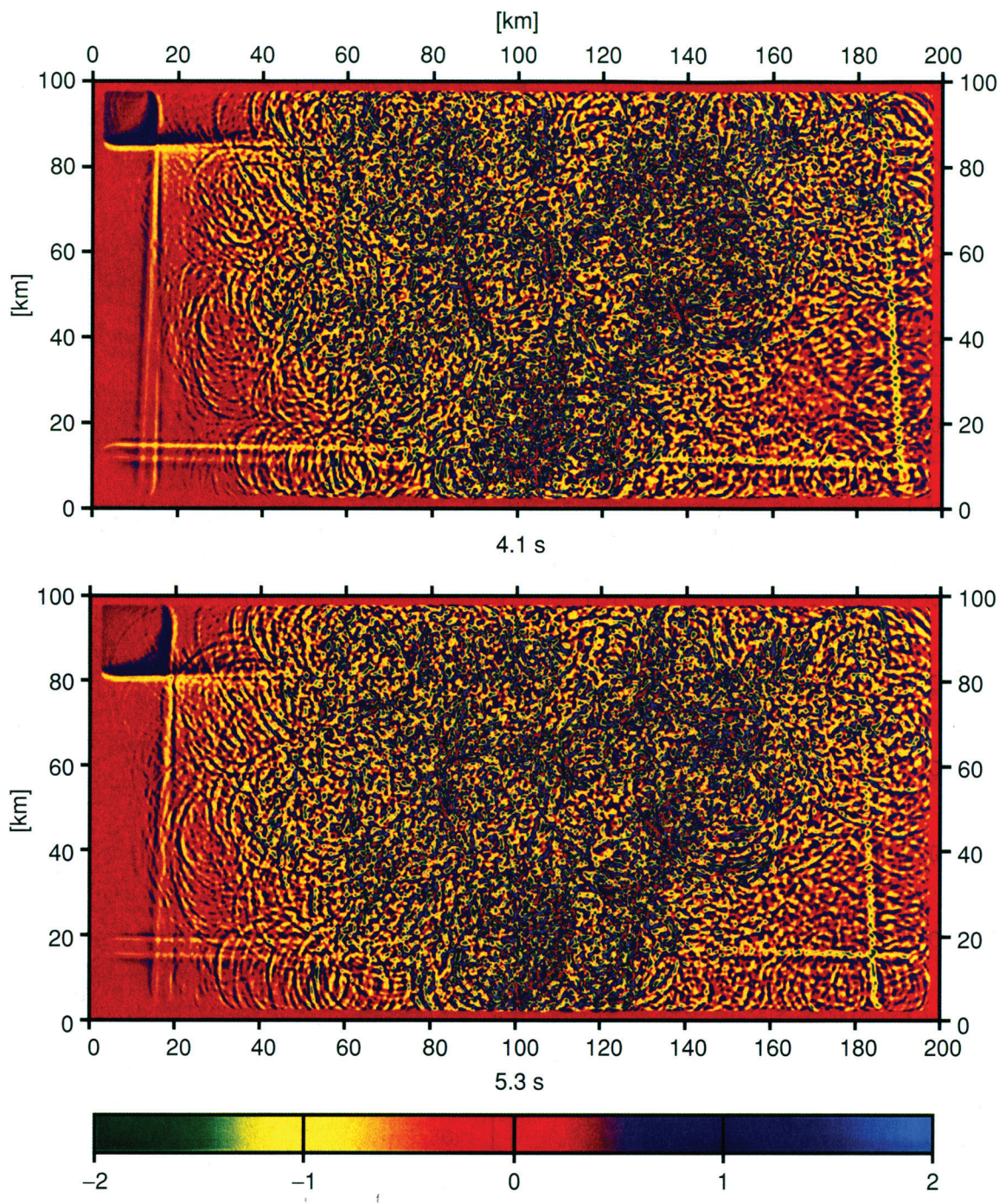


Figure 3 As Fig. 2, at times 4.1 s and 5.3 s after initial excitation of the plane wave.

CONCLUSIONS

New derivations of exact boundary conditions for free-surface topography on top of seismic media for wave propagation modelling are given and shown to be equivalent, both

mathematically and numerically, to boundary condition formulations derived in earlier work. We outline a numerical discretization by spatially second-order FDs of the boundary conditions, and show that the resulting system of equations for the free-surface particle velocities is spatially

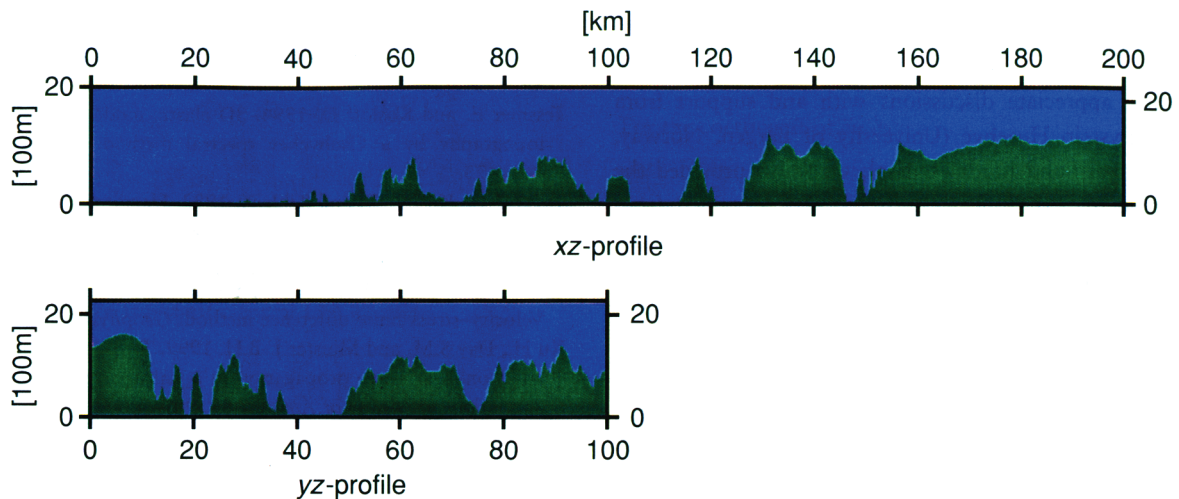


Figure 4 Vertically exaggerated (10 times) topographic west–east profile (upper plot) and south–north profile (lower plot), each at the middle of the domain covered by the surface of Fig. 1. Horizontal axes are in kilometres and vertical axes are in 100 m.

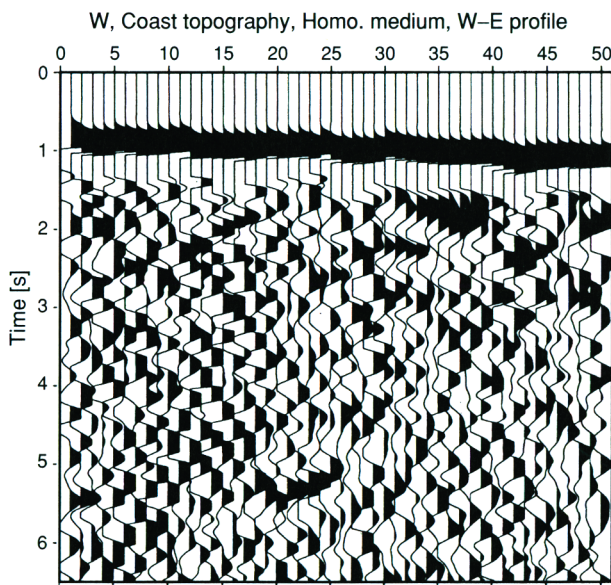


Figure 5 Seismogram of the vertical particle velocity component w for the viscoelastic simulation of Figs 2 and 3 along the west–east orientated profile of Fig. 4. The receivers are located from 76 to 125 km, at intervals of 1 km.

unconditionally stable. The boundary conditions are used in this work to propagate waves in full viscoelastic media using the velocity–stress formulation of the wave equations for curved grids. Our implementation gives realistic scattering and complex wave patterns due to out-of-plane effects from 3D topography. P-to-Rg scattering from mountainous areas is synthesized for an incident dipping plane P-wavefront on a fjord landscape of southwestern Norway. Fjords,

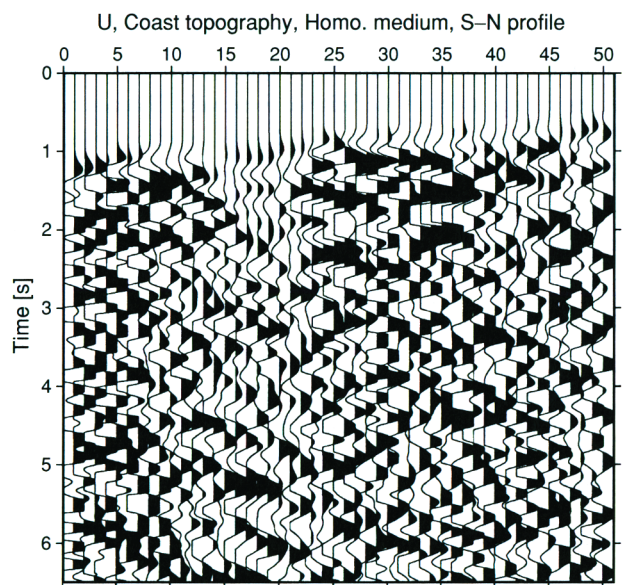


Figure 6 Seismogram of the horizontal particle velocity component u for the viscoelastic simulation of Figs 2 and 3 along the south–north orientated profile of Fig. 4. The receivers are located from 26 to 75 km, at intervals of 1 km.

simulated as valleys, are seen to exhibit attenuated higher frequency and amplified lower frequency transmitted and reflected waves. Many theoretical and numerical results predict amplitude amplification at ridge crests, but underestimate amplifications observed in the field. An explanation for this may be that these calculations assume 2D topographic geometries, ignoring out-of-plane effects (Hestholm *et al.* 1999).

ACKNOWLEDGEMENTS

We greatly appreciate discussions with and support from Professor Eystein Husebye (University of Bergen, Norway, Department of Solid Earth Physics), who also provided the topographic map of southwestern Norway, obtained from the Norwegian Governmental Map Authorities. We thank Professor Manik Talwani (Rice University) and Professor George McMechan (University of Texas at Dallas) for support, as well as Liz Henderson (Earth Resources Laboratory, MIT) and two anonymous reviewers for useful comments that improved the manuscript. This research was supported by the Norwegian Research Council and by the Earth Resources Laboratory, MIT, both through postdoctoral fellowships. The research was also supported by the Cold Regions Research and Engineering Laboratory, US Army Corps of Engineers, under contract DACA89-99-C-0002, the Norwegian Defense Research Establishment under contract FFI-0070, and by the Norwegian Supercomputer Committee through a grant of computing time. B.R. acknowledges the sponsors of the Seismic Reservoir Characterization (SRC) Project (Enterprise Oil, Norsk Hydro, PGS, Saga Petroleum and Statoil) at the University of Bergen. This paper is Contribution No. 983 from the Department of Geosciences at the University of Texas at Dallas.

REFERENCES

- Blanch J.O., Robertsson J.O.A. and Symes W.W. 1995. Modeling of a constant Q: Methodology and algorithm for an efficient and optimally inexpensive viscoelastic technique. *Geophysics* 60, 176–184.
- Fornberg B. 1988a. Generation of finite difference formulas on arbitrary spaced grids. *Mathematics of Computation* 51, 699–706.
- Fornberg B. 1988b. The pseudospectral method: Accurate representation of interfaces in elastic wave calculations. *Geophysics* 53, 625–637.
- Gottschämmer E. and Olsen K.B. 2001. Accuracy of the explicit planar free-surface boundary condition implemented in a fourth-order staggered-grid velocity–stress finite-difference scheme. *Bulletin of the Seismological Society of America* 91, 617–623.
- Hestholm S.O. 1999. 3-D finite difference viscoelastic wave modeling including surface topography. *Geophysical Journal International* 139, 852–878.
- Hestholm S.O., Ruud B.O. and Husebye E.S. 1999. 3-D versus 2-D finite difference seismic synthetics including real surface topography. *Physics of the Earth and Planetary Interiors* 113, 339–354.
- Levander A.R. 1988. Fourth-order finite-difference P-SV seismograms. *Geophysics* 53, 1425–1436.
- Robertsson J.O.A. 1996. A numerical free-surface condition for elastic-viscoelastic finite-difference modeling in the presence of topography. *Geophysics* 61, 1921–1934.
- Ruud B.O. and Hestholm S.O. 2001. 2D surface topography boundary conditions in seismic wave modelling. *Geophysical Prospecting* 49, 445–460.
- Tessmer E. and Kosloff D. 1994. 3D elastic modeling with surface topography by a Chebychev spectral method. *Geophysics* 59, 464–473.
- Tessmer E., Kosloff D. and Behle A. 1992. Elastic wave propagation simulation in the presence of surface topography. *Geophysical Journal International* 108, 621–632.
- Virieux J. 1986. P-SV wave propagation in heterogeneous media: Velocity–stress finite-difference method. *Geophysics* 51, 889–901.
- Xu H., Day S.M. and Minster J.-B.H. 1999. Two-dimensional linear and nonlinear wave propagation in a half-space. *Bulletin of the Seismological Society of America* 89, 903–917.

APPENDIX

Equivalence of boundary condition formulations

Using definitions (17)–(21) and

$$q \equiv \cos[\arctan(p)] = \cos \phi, \quad (\text{A1})$$

$$r \equiv \sin[\arctan(p)] = \sin \phi, \quad (\text{A2})$$

where ϕ is the second slope angle of the local topography, we multiply the last of the new boundary condition formulations (equation (26)) by d and add the result to the first (equation (24)). Some simple algebra gives

$$\begin{aligned} & \left[d^2(1 - \zeta) + \left(1 + \frac{p^2}{e^2} \right)(1 - \zeta) \right] C(\xi, \kappa) \frac{\partial u}{\partial \eta} \\ & + d \left[(1 + d^2)(1 - \zeta) + \frac{p^2}{e^2}(1 - \zeta) \right] C(\xi, \kappa) \frac{\partial w}{\partial \eta} \\ & = (1 - \zeta) \left[2d \frac{\partial u}{\partial \xi} + \frac{p}{e} \frac{\partial v}{\partial \xi} + (d^2 - 1) \frac{\partial w}{\partial \xi} + \frac{p}{e} \frac{\partial u}{\partial \kappa} + \frac{dp}{e} \frac{\partial w}{\partial \kappa} \right]. \quad (\text{A3}) \end{aligned}$$

Using the trigonometric identity

$$d^2 + 1 + \frac{p^2}{e^2} = \frac{1}{e^2} + \frac{p^2}{e^2} = \frac{1}{e^2}(1 + p^2), \quad (\text{A4})$$

and dividing through by $(1 - \zeta)$ (thereby assuming $\mu \neq 0$), gives (27).

To arrive at (28) from (24)–(26), we multiply equation (26) by ep , add (25), and subtract (24) after multiplying it by dep ; in other words $ep \times (26) + (25) - dep \times (24)$, where the numbers refer to equations. This gives, after some terms cancel out,

$$\begin{aligned} & \left(-2dep + \frac{dp}{e} \zeta + \frac{dp}{e} - 2d^3 ep - \frac{d}{e} p^3 + \frac{d}{e} p^3 \zeta \right) C(\xi, \kappa) \frac{\partial u}{\partial \eta} \\ & + \left(-p^2 - p^2 \zeta + d^2 - d^2 \zeta + 1 - \zeta + 2 \frac{p^2}{e^2} - d^2 p^2 - d^2 p^2 \zeta \right) C(\xi, \kappa) \frac{\partial v}{\partial \eta} \\ & + \left(2ep + 2d^2 ep + \frac{p^3}{e} - \frac{p^3}{e} \zeta - \frac{p}{e} - \frac{p}{e} \zeta \right) C(\xi, \kappa) \frac{\partial w}{\partial \eta} \end{aligned}$$

$$\begin{aligned}
&= \left(-2ep\zeta + 2\frac{p}{e}\zeta - 2d^2ep \right) \frac{\partial u}{\partial \xi} + (d - d\zeta - dp^2 + dp^2\zeta) \frac{\partial v}{\partial \xi} \\
&\quad + (2dep - 2dep\zeta) \frac{\partial w}{\partial \xi} + (d - d\zeta - dp^2 + dp^2\zeta) \frac{\partial u}{\partial \kappa} \\
&\quad + \left(-2ep\zeta + 2\frac{p}{e} - 2d^2ep\zeta \right) \frac{\partial v}{\partial \kappa} + (p^2 - p^2\zeta - 1 + \zeta) \frac{\partial w}{\partial \kappa}.
\end{aligned} \tag{A5}$$

Now we simplify each of the coefficients by using trigonometric identities. For the coefficient of $C(\xi, \kappa)\partial u/\partial \eta$:

$$\begin{aligned}
&dep \left(-2 + \frac{1}{e^2}\zeta + \frac{1}{e^2} - 2d^2 - \frac{p^2}{e^2} + \frac{p^2}{e^2}\zeta \right) \\
&= fp \left[-2(1 + d^2) + \frac{1}{e^2}(1 - p^2 + \zeta + p^2\zeta) \right] \\
&= \frac{fp}{e^2} [-2 + 1 - p^2 + \zeta(1 + p^2)] \\
&= -\frac{fp}{e^2} [(1 + p^2)(1 - \zeta)],
\end{aligned} \tag{A6}$$

noting that $1+d^2=1/e^2$ and $de=f$. For the coefficient of $C(\xi, \kappa)\partial v/\partial \eta$:

$$\begin{aligned}
&-p^2 \left(1 + d^2 + \zeta + d^2\zeta - \frac{2}{e^2} \right) + (1 - \zeta)(1 + d^2) \\
&= -p^2 \left[(1 + d^2)(1 + \zeta) - \frac{2}{e^2} \right] + (1 - \zeta)(1 + d^2) \\
&= -p^2 \left(\frac{1}{e^2} + \frac{\zeta}{e^2} - \frac{2}{e^2} \right) + (1 - \zeta) \frac{1}{e^2} \\
&= -\frac{p^2}{e^2} (-1 + \zeta) + \frac{1}{e^2}(1 - \zeta) \\
&= \frac{1}{e^2}(1 + p^2)(1 - \zeta).
\end{aligned} \tag{A7}$$

For the coefficient of $C(\xi, \kappa)\partial w/\partial \eta$:

$$\begin{aligned}
&\frac{p}{e}(2e^2 + 2d^2e^2 + p^2 - p^2\zeta - 1 - \zeta) \\
&= \frac{p}{e}[2e^2 + 2f^2 + p^2(1 - \zeta) - 1 - \zeta] \\
&= \frac{p}{e}(1 + p^2)(1 - \zeta).
\end{aligned} \tag{A8}$$

For the coefficient of $\partial u/\partial \xi$:

$$\begin{aligned}
&-2dfp \left(\frac{e\zeta}{df} - \frac{\zeta}{def} + \frac{de}{f} \right) = -2dfp \left(\frac{\zeta}{d^2} - \frac{\zeta}{f^2} + 1 \right) \\
&= -2dfp \left[\zeta \left(\frac{e^2 - 1}{f^2} \right) + 1 \right] \\
&= -2dfp(1 - \zeta).
\end{aligned} \tag{A9}$$

For the coefficient of $\partial v/\partial \xi$:

$$d(1 - \zeta) - dp^2(1 - \zeta) = d(1 - p^2)(1 - \zeta). \tag{A10}$$

For the coefficient of $\partial w/\partial \xi$:

$$2dep - 2dep\zeta = 2fp(1 - \zeta). \tag{A11}$$

For the coefficient of $\partial u/\partial \kappa$:

$$d[(1 - p^2) - \zeta + p^2\zeta] = d(1 - p^2)(1 - \zeta). \tag{A12}$$

For the coefficient of $\partial v/\partial \kappa$:

$$2\frac{p}{e}(1 - e^2\zeta - d^2e^2\zeta) = 2\frac{p}{e}[1 - \zeta(e^2 + f^2)] = 2\frac{p}{e}(1 - \zeta). \tag{A13}$$

For the coefficient of $\partial w/\partial \kappa$:

$$p^2 - p^2\zeta - 1 + \zeta = (p^2 - 1)(1 - \zeta). \tag{A14}$$

The equation resulting from these trigonometric simplifications is divided through by $(1 - \zeta)$, giving (28).

To get (29) from (24)–(26), we take (26), subtract $d \times (24)$ before subtracting $p/e \times (25)$; in other words $(26) - d \times (24) - p/e \times (25)$. This gives

$$\begin{aligned}
&d \left[-\zeta - 1 - 2d^2 - \left(1 + \frac{p^2}{e^2} \right)(1 - \zeta) - \frac{p^2}{e^2}\zeta - \frac{p^2}{e^2} \right] C(\xi, \kappa) \frac{\partial u}{\partial \eta} \\
&+ \frac{p}{e} \left[-\zeta - 1 - d^2\zeta - d^2 - (1 + d^2)(1 - \zeta) - 2\frac{p^2}{e^2} \right] C(\xi, \kappa) \frac{\partial v}{\partial \eta} \\
&+ \left[2 + \left(d^2 + \frac{p^2}{e^2} \right)(1 - \zeta) + d^2\zeta + d^2 + \frac{p^2}{e^2}\zeta + \frac{p^2}{e^2} \right] C(\xi, \kappa) \frac{\partial w}{\partial \eta} \\
&= \left(-2\zeta - 2d^2 - 2\frac{p^2}{e^2}\zeta \right) \frac{\partial u}{\partial \xi} - 2\frac{dp}{e}(1 - \zeta) \frac{\partial v}{\partial \xi} + 2d(1 - \zeta) \frac{\partial w}{\partial \xi} \\
&- 2\frac{dp}{e}(1 - \zeta) \frac{\partial u}{\partial \kappa} + \left(-2\zeta - 2d^2\zeta - 2\frac{p^2}{e^2} \right) \frac{\partial v}{\partial \kappa} + 2\frac{p}{e}(1 - \zeta) \frac{\partial w}{\partial \kappa}.
\end{aligned} \tag{A15}$$

We perform the following trigonometric simplifications. For the coefficient of $C(\xi, \kappa)\partial u/\partial \eta$:

$$\begin{aligned}
&d \left[\left(1 + \frac{p^2}{e^2} \right)(\zeta - 1) - \zeta \left(1 + \frac{p^2}{e^2} \right) - \left(1 + \frac{p^2}{e^2} + 2d^2 \right) \right] \\
&= d \left[\zeta \left(1 + \frac{p^2}{e^2} \right) - \left(1 + \frac{p^2}{e^2} \right) - \zeta \left(1 + \frac{p^2}{e^2} \right) - \left(1 + \frac{p^2}{e^2} \right) - 2d^2 \right] \\
&= -2d \left(1 + \frac{p^2}{e^2} + d^2 \right) = -2\frac{d}{e^2}(1 + p^2).
\end{aligned} \tag{A16}$$

For the coefficient of $C(\xi, \kappa)\partial v/\partial \eta$:

$$\begin{aligned}
&\frac{p}{e} \left[-(1 + d^2)(1 + \zeta) - (1 + d^2)(1 - \zeta) - 2\frac{p^2}{e^2} \right] \\
&= \frac{p}{e} \left[-(1 + d^2)(1 + \zeta + 1 - \zeta) - 2\frac{p^2}{e^2} \right] = -2\frac{p}{e} \left(1 + d^2 + \frac{p^2}{e^2} \right) \\
&= -2\frac{p}{e} \frac{1}{e^2}(1 + p^2) = -2\frac{p}{e^3}(1 + p^2).
\end{aligned} \tag{A17}$$

For the coefficient of $C(\zeta, \kappa) \partial w / \partial \eta$:

$$\begin{aligned} & \left[2 + \left(d^2 + \frac{p^2}{e^2} \right) (1 - \zeta) + \left(d^2 + \frac{p^2}{e^2} \right) (\zeta + 1) \right] \\ &= 2 + \left(d^2 + \frac{p^2}{e^2} \right) (1 - \zeta + \zeta + 1) \\ &= 2 \left(1 + d^2 + \frac{p^2}{e^2} \right) = \frac{2}{e^2} (1 + p^2). \end{aligned} \quad (\text{A18})$$

For the coefficient of $\partial u / \partial \xi$:

$$\left(-2\zeta - 2d^2 - 2\frac{p^2}{e^2}\zeta \right) = -2 \left[\zeta \left(1 + \frac{p^2}{e^2} \right) + d^2 \right]. \quad (\text{A19})$$

For the coefficient of $\partial v / \partial \kappa$:

$$-2 \left[\zeta (1 + d^2) + \frac{p^2}{e^2} \right] = -\frac{2}{e^2} (\zeta + p^2). \quad (\text{A20})$$

Dividing through the resulting equation by -2 gives (29).

It is also possible to obtain the same result by using the boundary conditions (26) and (27) directly. This is done in the following. The boundary condition (26) gives

$$w(\zeta, \kappa) = \frac{1}{e^2} (1 + p^2) \quad \text{at } \zeta = 0, \quad (\text{A21})$$

and the boundary condition (27) gives

$$w(\zeta, \kappa) = \frac{1}{e^2} (1 + p^2) \quad \text{at } \zeta = 1. \quad (\text{A22})$$

Subtracting (A21) from (A22) gives

$$w(\zeta, \kappa) = \frac{1}{e^2} (1 + p^2) \quad \text{at } \zeta = 1 - \kappa. \quad (\text{A23})$$

Substituting (A23) into the expression for w given by (A17) gives

$$w(\zeta, \kappa) = \frac{1}{e^2} (1 + p^2) \quad \text{at } \zeta = 1 - \kappa. \quad (\text{A24})$$

Substituting (A24) into the expression for w given by (A17) gives

$$w(\zeta, \kappa) = \frac{1}{e^2} (1 + p^2) \quad \text{at } \zeta = 1 - \kappa. \quad (\text{A25})$$

Substituting (A25) into the expression for w given by (A17) gives

$$w(\zeta, \kappa) = \frac{1}{e^2} (1 + p^2) \quad \text{at } \zeta = 1 - \kappa. \quad (\text{A26})$$

Substituting (A26) into the expression for w given by (A17) gives

$$w(\zeta, \kappa) = \frac{1}{e^2} (1 + p^2) \quad \text{at } \zeta = 1 - \kappa. \quad (\text{A27})$$

Substituting (A27) into the expression for w given by (A17) gives

$$w(\zeta, \kappa) = \frac{1}{e^2} (1 + p^2) \quad \text{at } \zeta = 1 - \kappa. \quad (\text{A28})$$

Substituting (A28) into the expression for w given by (A17) gives

$$w(\zeta, \kappa) = \frac{1}{e^2} (1 + p^2) \quad \text{at } \zeta = 1 - \kappa. \quad (\text{A29})$$

Substituting (A29) into the expression for w given by (A17) gives

$$w(\zeta, \kappa) = \frac{1}{e^2} (1 + p^2) \quad \text{at } \zeta = 1 - \kappa. \quad (\text{A30})$$

Substituting (A30) into the expression for w given by (A17) gives

$$w(\zeta, \kappa) = \frac{1}{e^2} (1 + p^2) \quad \text{at } \zeta = 1 - \kappa. \quad (\text{A31})$$

Substituting (A31) into the expression for w given by (A17) gives

$$w(\zeta, \kappa) = \frac{1}{e^2} (1 + p^2) \quad \text{at } \zeta = 1 - \kappa. \quad (\text{A32})$$

Substituting (A32) into the expression for w given by (A17) gives

$$w(\zeta, \kappa) = \frac{1}{e^2} (1 + p^2) \quad \text{at } \zeta = 1 - \kappa. \quad (\text{A33})$$

Substituting (A33) into the expression for w given by (A17) gives

$$w(\zeta, \kappa) = \frac{1}{e^2} (1 + p^2) \quad \text{at } \zeta = 1 - \kappa. \quad (\text{A34})$$